Supporting Information

Identification of the valence and coordination environment of the particulate methane monooxygenase copper centers by advanced EPR characterization

Megen A. Culpepper,[‡] George E. Cutsail III,[‡] William A. Gunderson, Brian M. Hoffman,[*] and Amy C. Rosenzweig[*]

Departments of Molecular Biosciences and of Chemistry, Northwestern University, Evanston, IL 60208, United States

[‡]These two authors contributed equally to this work.

Table S1. Summary of pMMO copper analysis

	Monocopper site	Type of EPR sample	Total copper (per protomer)	EPR quantitation (per protomer)	Reference
Methylococcus capsulatus (Bath)	Yes	Purified	2.7 ± 0.1	1.4 ± 0.3	1*
		Purified	2.4 ± 0.1	~1.0 – 1.4	2
		Membrane-bound	20 ± 3	4 ± 1	3
		Membrane-bound	~ 15	1.6 ± 0.2 (3K)/1.7 ± 0.4 (77K)	4
		Purified	2.4	0.6 – 0.8	5
Methylococcus capsulatus (strain M)	Yes	Membrane-bound	2.25 – 3	0.5 – 1	6
Methylomicrobium album (BG8)	Yes	Membrane-bound	3.4 – 4.6	1.2 – 1.4	7
Methylocystis species (strain M)	No	Membrane-bound	2.3 ± 0.2	~ 1.6	8
		Solubilized	2.1 ± 0.5	~ 0.8	
Methylosinus trichosporium OB3b	No	Membrane-bound	4.8 ± 1.1	~ 4.7	9
		Solubilized	4.0 ± 1.1	2.9 – 4.8	
		Purified	1.4 ± 0.6	~1.2	
		Membrane-bound	~ 6	~1.6	10

*Reported value is normalized against the spmoB_penta variant.

Table S2. Summary of EPR quantitation from this work*

	Dicopper Site	Monocopper Site	Type of EPR Sample	Total Copper	EPR quantitation
M. capsulatus (Bath) pMMO	Yes	Yes	Purified	2.9 ± 0.2	1.6 ± 0.4
spmoB_wt	Yes	Yes	Purified	2.8 ± 0.4	2.0 ± 0.6
spmoB_H48N,H72A	Yes	No	Purified	2.0 ± 0.3	1.8 ± 0.3
spmoB_H33,137,139A	No	Yes	Purified	0.9 ± 0.1	0.5 ± 0.2
spmoB_penta	No	No	Purified	0.2 ± 0.1	0.2 ± 0.1

*Absolute values reported. No normalization against the spmoB_penta variant.

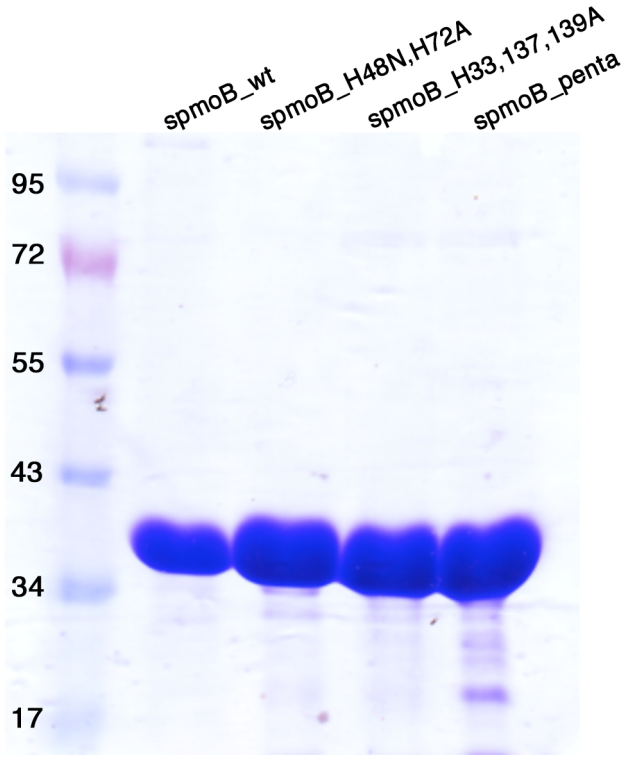

Figure S1. SDS-PAGE gel of spmoB_wt and variants purified from BL21(DE3) *E. coli* inclusion bodies. Inclusion bodies were solubilized in buffer containing 1% Triton X-100, then washed in buffer without Triton X-100 and denatured in 8 M urea. The purified inclusion bodies were refolded in the presence of 1 mM $CuSO_4$ by stepwise dilutions to reduce the urea concentration.

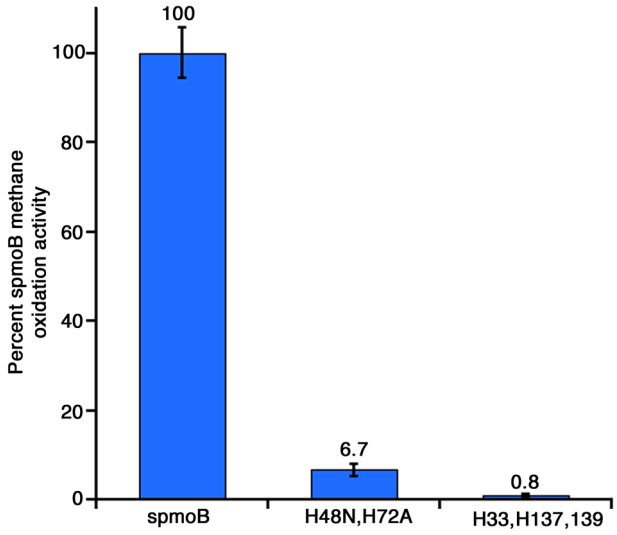

Figure S2. Methane oxidation activity of spmoB and variants. The formation of methanol was detected by gas chromatography. Activity is reported as percent of spmoB_wt methane oxidation activity (22.3 ± 5.7 nmol methanol μmol^{-1} min^{-1}). Error bars represent an average of six activity assays. The only variant to yield any detectable activity is spmoB_H48N,H72A, which is consistent with previously reported results.

^{14}N PESTRE analysis

Experimental:

PESTRE allows one to determine the sign of A/g_n, and is a multicomponent protocol composed of three different stages of Davies ENDOR sequences. The RF pulse is not applied during the first set of sequences of the PESTRE trace, thus saturating the EPR signal and establishing the baseline signal level (BSL). In the next set of sequences, a single RF frequency is applied during the Davies ENDOR experiment and is driven towards ENDOR saturation. The RF is then turned off during the final set of Davies sequences of the PESTRE trace, and the spin-echo EPR response, denoted the 'dynamic reference level' (DRL), and relaxes back to the BSL. The sign of the difference as the DRL relaxes to the BSL, DRLδ = DRL - BSL, determines the absolute sign of A/g_n.

Results:

^{14}N Davies ENDOR responses at g ~2.15 for the EPR-active Cu(II) assigned to the dinuclear copper sites of spmoB_wt and spmoB_H48N,H72A are nearly identical, with three distinct features at ~9.0, 15.5, and 22.5 MHz (Figure S3). These three features are assigned as the overlapping ν_+/ν_- branches of two ^{14}N, I = 1 ligands without resolved quadrupole coupling, one, denoted N1, with A = + 38 MHz according to Eq 1, the second, N*, with A = + 25 MHz, with the absolute hyperfine signs of A determined through a Pulsed ENDOR Saturation and Recovery (PESTRE) experiment (Figure S3).

The δDRL PESTRE response at each ν_+ transition at 15.5 and 22.5 MHz for spmoB_H48N,H72A is negative. The negative δDRL PESTRE response for each ν_+ transition indicates a positive spin density, $\rho > 0$ and a positive hyperfine coupling as $\rho \propto A/g_n$, where g_n is positive for ^{14}N. Two ENDOR transitions that have the same δDRL PESTRE response and are from nitrogen species would be a result of ^{14}N quadrupole splitting. However, a quadrupole splitting of $3P$ = 7 MHz is much large than associated with a histidine ^{14}N, so these hyperfine transitions at 15 and 22.5 MHz must belong to two different nitrogen species without resolved quadrupole splitting, termed N1 and N*. The stronger β δDRL PESTRE response of N*'s ν_+ transition dominates the weaker unobserved opposite α δDRL PESTRE response of N1's ν_- transition at 15.5 MHz. This phenomenon has been observed previously in the multi-iron PESTRE responses of nitrogenase.[11] The ν_- of N* at 9.0 MHz exhibits the expected opposite positive, α, δDRL PESTRE response of its ν_+ partner, confirming that N* assignment of A(N*) = +25 MHz.

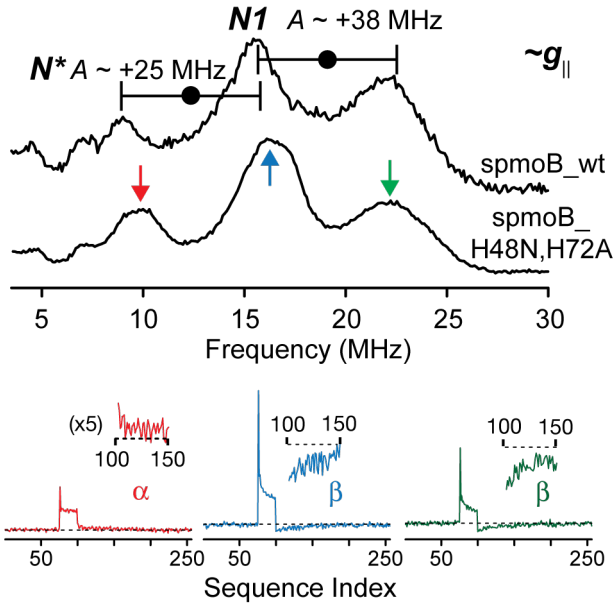

Figure S3. The 34.82 GHz ENDOR Davies traces (π = 80ns, τ = 600 ns, T = 20 μs, repetition rate = 20 ms) of spmoB_wt and spmoB_H48N,H72A, collected at 2 K and g = 2.15 (top) and PESTRE traces for spmoB_H48N,H72A (bottom). Each PESTRE trace is collected at the single RF frequency indicated by the corresponding color arrow on the ENDOR spectrum: 9.75 MHz, red; 16.10 MHz, blue; 22.10 MHz, green; BSL, sequences 1 – 75; RF on, seq: 76 – 100; DRL, seq: 101 – 256. The inset of each PESTRE trace is a relative expansion (x5) of the DRLδ with the respective BSL and not level along with the labeled α or β response. The intensities of all the PESTRE traces collectively have been expanded arbitrarily relative to the ENDOR trace for presentation.

^{14}N ESEEM analysis

Additional details of ESEEM simulation (Figure 6):

The simulation of the Cu(II)His_2 for spmoB_H48N,H72A(Figure 6, *red*) center includes a rotation of the A-tensor, representing the relative orientation between the two histidyl imidazoles. Since the data were only collected at a single magnetic field, there is no orientation with respect to the g-tensor ([α, β, γ]**A** = [0, 0, 0]). The A tensor of the second remote histidyl nitrogen is rotated approximately 120° from the other and represented by the Euler angles **A**[α, β, γ] = [240°, 65°, 0°]. This is indicative of an approximately tetrahedral geometry at the Cu(II) site,[1] similar to the modeling of His137 and His139 of the dicopper site in the crystal structure.[12] The double quantum feature (see results) confirms that these two imidazoles in spmoB_H48N,H72A are binding to the same Cu(II) center.

A Cu(II)His_2 simulation of pMMO was achieved with a similar hf and nqi parameters with a rotation between the two A-tensors matching spmoB_H48N,H72A: **A**[α, β, γ] = [240°, 70°, 0°]. As described in the results, the ESEEM response of pMMO is anticipated to have an additional Cu(II) ESEEM signal arising from the dicopper valence-scrambling. Examination of the crystal structure predicts ligation by His33 and the N-terminal amino group (Cu(II)His) and is separately simulated using the same hf and nqi parameters from the Cu(II)His_2 with no orientation with respect to the other (Figure S4, *blue*). This simulation alone does not fit the neither spmoB_H48N,H72A nor pMMO data well because of the lack of the double-quantum feature arising from two identical ligands for the same Cu(II) ion(Figure S4).

The averaged sum of the two pMMO Cu(II) ESEEM simulations, Cu(II)His_2 (A) and Cu(II)His (B), does fit the data (Figure 4S, *purple*). The addition of the second Cu(II) center with a single histidine ligand in the summed spectrum does not exhibit any significant changes (1/2A+1/2B) from A, for both the time-domain and frequency-domain. The summed spectrum retains the double quantum feature at approximately 8 MHz, confirming the Cu(II)His_2 is present, as in spmoB_H48N,H72A. Therefore, one location of the dicopper center is distinctly characterized in spmoB_H48N,H72A. Both copper locations are occupied by and characterized in the valance-scrambled pMMO dicopper center which has the spectral features of spmoB_H48N,H72A (H137, H139) and a Cu(II) coordinated by His33 and an amino group.

Table S3. Simulation parameters

	spmoB_H48N,H72A		pMMO	
	Cu(II)His_2 (A)	Cu(II)His (B)	Cu(II)His_2 (A)	Cu(II)His (B)
A (MHz)	[1.57, 1.07, 2.03]	[1.57, 1.07, 2.03]	[1.68, 1.18, 2.13]	[1.68, 1.18, 2.13]
e^2Qq (MHz)	1.51	1.51	1.53	1.53
η	0.91	0.91	0.87	0.87
A[α, β, γ]°	[240, 70, 0]	–	[240, 65, 0]	–
Q[α, β, γ]°	[0,55,0]	–	[0, 60, 0]	–

Table S4. χ^2 parameters for ESEEM simulations

	spmoB_H48N,H72A	pMMO
Cu(II)His	125.7	115.7
Cu(II)His_2	78.3	60.6
1/2(Cu(II)His_1+Cu(II)His_2)	—	46.5

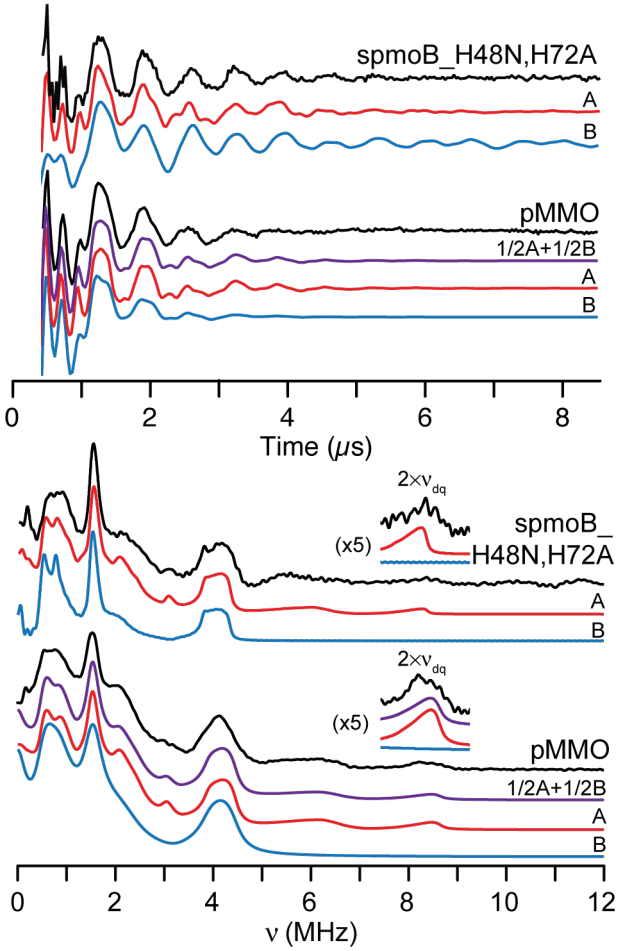

Figure S4. Three-pulse ESEEM time-domain waveforms (top) and Fourier transformed frequency-domain spectra for spmoB_H48N,H72A and *M. capsulatus* (Bath) pMMO in black. Simulations: A = Cu(II)His_2, *red*; B = Cu(II)His, *blue*; 1/2A+1/2B, *purple*. The $2\upsilon_{dq}$ combination features of the frequency-domain spectra are expanded five times as insets. Parameters given in Table S3. Spectral conditions for spmoB_H48N, H72A: ν_{mw} = 9.72 GHz, B_0 = 3390 G, τ = 348 ns, T_0 = 32 ns, ΔT = 32 ns, 256 points. Spectral conditions for pMMO: same as spmoB_H48N72A except B_0 = 3375 G.

REFERENCES

(1) This work.
(2) Lieberman, R. L.; Shrestha, D. B.; Doan, P. E.; Hoffman, B. M.; Stemmler, T. L.; Rosenzweig, A. C. *Proc. Natl. Acad. Sci. USA* **2003**, *100*, 3820.
(3) Nguyen, H. T.; Nakagawa, K. H.; Hedman, B.; Elliott, S. J.; Lidstrom, M. E.; Hodgson, K. O.; Chan, S. I. *J. Am. Chem. Soc.* **1996**, *118*, 12766.
(4) Hung, S.-C.; Chen, C.-L.; Chen, K. H.-C.; Yu, S. S.-F.; Chan, S. I. *J. Chin. Chem. Soc.* **2004**, *51*, 1229.
(5) Basu, P.; Katterle, B.; Andersson, K. K.; Dalton, H. *Biochem. J.* **2003**, *369*, 417.
(6) Katterle, B.; Gvozdev, R. I.; Abudu, N.; Ljones, T.; Andersson, K. K. *Biochem. J.* **2002**, *363*, 677.
(7) Yuan, H.; Collins, M. L.; Antholine, W. E. *J. Inorg. Biochem.* **1998**, *72*, 179.
(8) Smith, S. M.; Rawat, S.; Telser, J.; Hoffman, B. M.; Stemmler, T. L.; Rosenzweig, A. C. *Biochemistry* **2011**, *50*, 10231.
(9) Hakemian, A. S.; Kondapalli, K. C.; Telser, J.; Hoffman, B. M.; Stemmler, T. L.; Rosenzweig, A. C. *Biochemistry* **2008**, *47*, 6793.
(10) Takeguchi, M.; Miyakawa, K.; Okura, I. *J. Mol. Cat. A: Chem* **1999**, *137*, 161.
(11) Doan, P. E.; Telser, J.; Barney, B. M.; Igarashi, R. Y.; Dean, D. R.; Seefeldt, L. C.; Hoffman, B. M. *J. Am. Chem. Soc.* **2011**, *133*, 17329.
(12) Lieberman, R. L.; Rosenzweig, A. C. *Nature* **2005**, *434*, 177.